Elemental segregation in CoCrFeMnNi high entropy alloy after intermediate-temperature low cycle fatigue loading

Dimitri Litvinov [*,1], Kaiju Lu [1], Mario Walter, Jarir Aktaa

Institute for Applied Materials, Karlsruhe Institute of Technology (KIT), Eggenstein-Leopoldshafen 76344, Germany

Keywords:
High entropy alloy
Fatigue
Transmission electron microscopy
Dislocation
Intermediate-temperature

A B S T R A C T

We report on the elemental segregation in CoCrFeMnNi high entropy alloy after low cycle fatigue loading at 550 °C via transmission electron microscopy. The segregation of Fe, Co and Ni elements at the grain boundaries was identified, which is in addition to previously reported precipitation of MnNi-rich and Cr-rich phases. Besides, cyclic straining is suggested to play an assisting role in the precipitation of these phases and the elemental segregation upon cycling CoCrFeMnNi at intermediate temperatures. In addition, various dislocation patterns in the post-fatigued CoCrFeMnNi are compared to those in monotonic loading.

1. Introduction

In the past two decades the equiatomic CoCrFeMnNi high entropy alloy (HEA), first reported by Cantor et al. [1], has been extensively studied. The so-called Cantor alloy has face-centered cubic (FCC) structure and shows high strength, excellent ductility, and sufficient fracture toughness [2–4]. Previous investigations on CoCrFeMnNi have shown an interplay of various crystal defects, such as dislocations, twins and stacking faults, during plastic deformation depending on several factors: temperature, grain size and orientation, loading direction (tensile or compressive) and strain level [5–13]. For instance, Zhang et al. reported that partial and full dislocations dominate the deformation in CoCrFeMnNi at room temperature [6]. The presence of partial dislocations has been attributed to the low-to-medium stacking fault energy (SFE) of CoCrFeMnNi at room temperature [7]. For example, the SFE of CoCrFeMnNi is ~21 mJ/m^2 at room temperature according to the *ab initio* calculations [14]. Furthermore, deformation twinning was observed in the CoCrFeMnNi HEA at cryogenic temperatures and contributed to the enhanced strength and ductility [5]. Later on, deformation twins were also found in coarse-grained CoCrFeMnNi alloy after tensile deformation at room temperature [13].

Despite these studies focusing on the monotonic deformation features of CoCrFeMnNi alloy, there is still no comprehensive investigation comparing the microstructure evolution of CoCrFeMnNi HEA upon cyclic deformation and monotonic deformation at intermediate temperatures, which is critical for the HEA's intermediate-temperature applications. Besides, it has been reported that Cr- and NiMn-enriched secondary phases formed upon cycling CoCrFeMnNi at 550 °C [15,16], however, their detailed crystal structures and the role of cyclic straining on their formation were not identified yet. Consequently, this work intends to extensively investigate the microstructure of CoCrFeMnNi HEA after low-cycle fatigue (LCF) loading at 550 °C by transmission electron microscopy (TEM).

2. Material and experimental techniques

The investigated equiatomic CoCrFeMnNi was synthesized using arc melting, followed by drop-casting, homogenization and rotary swaging [4,15]. The LCF specimens were machined out of the rotary-swaged material and finally recrystallized by annealing at 800 °C for 1 h, leading to a refined isotropic microstructure [15].

LCF tests were carried out at 550 °C with strain amplitudes ranging from ± 0.2% to ± 0.75% under a symmetric triangular waveform and at a nominal strain rate of 3×10^{-3} s^{-1} on a MTS 810 servo-hydraulic testing machine equipped with a radiative furnace and a high-temperature extensometer. The specimen geometry includes a gauge diameter of 2 mm, and a gauge length of 7.6 mm. It should be mentioned that the lifetime and cyclic stress response of this material under LCF loading at 550 °C have been reported in Ref. [15].

To investigate the post-fractured microstructures, TEM investigations were carried out using TECNAI-20 F and Talos F200X microscopes equipped with the high-angle annular dark-field (HAADF)

* Corresponding author.
E-mail address: litvinov@kit.edu (D. Litvinov).
[1] These authors contributed equally

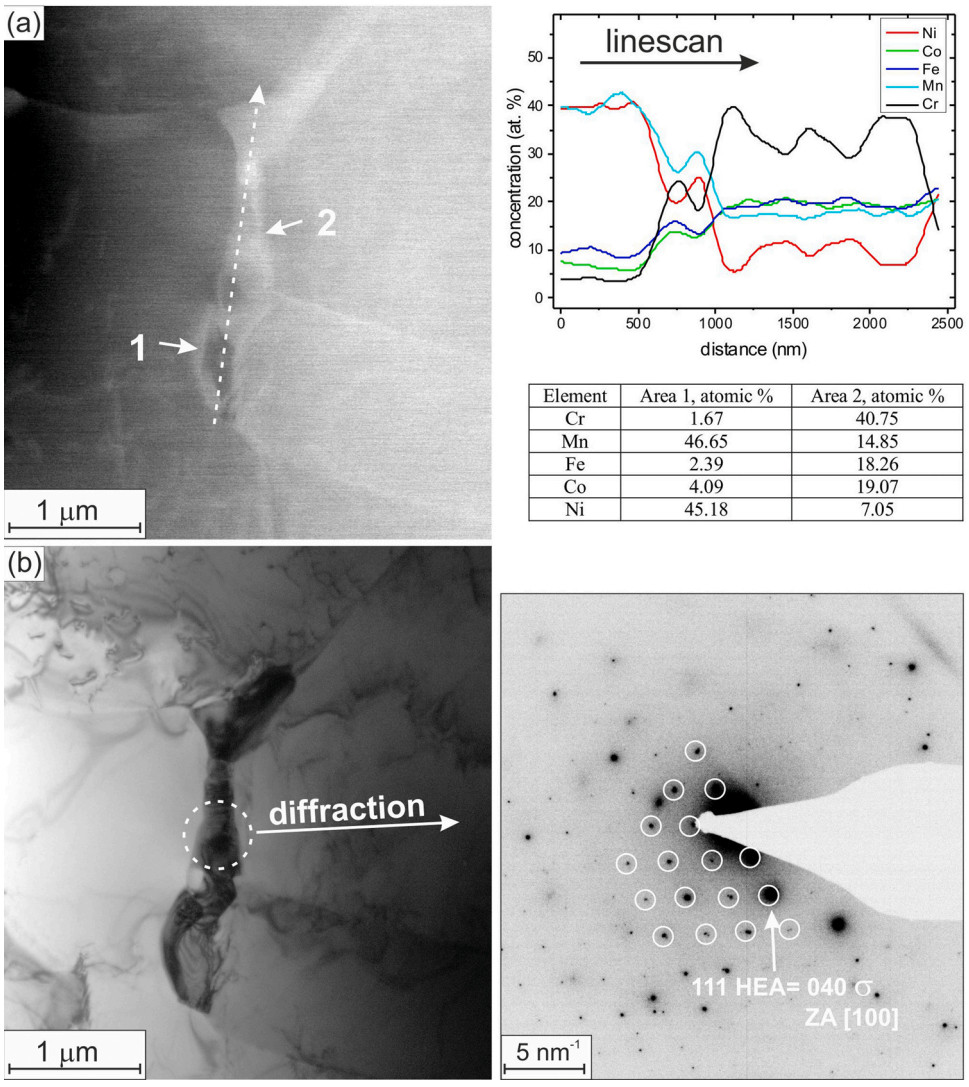

Element	Area 1, atomic %	Area 2, atomic %
Cr	1.67	40.75
Mn	46.65	14.85
Fe	2.39	18.26
Co	4.09	19.07
Ni	45.18	7.05

Fig. 1. (a) HAADF STEM image with EDX line scan along the dashed arrow and elemental compositional measurements and (b) bright-field TEM image with SADP of circled areas of the same region of the sample tested under strain amplitude of ± 0.3%.

detector for scanning TEM (STEM). Energy-dispersive X-ray (EDX) spectroscopy was employed for the determination of elemental composition. Conventional TEM with selected area diffraction pattern (SADP) and high-resolution TEM (HRTEM) with fast Fourier transformation (diffractogram) analysis were also applied. For preparing TEM samples, the details can be found in Ref. [15].

To further reveal the role of cyclic straining on the secondary phases formation, additional TEM investigations were performed for an as-recrystallized specimen and a subsequently annealed specimen (at 550 °C for ~ 47 h, without fatigue loading). This duration of annealing (47 h) is chosen as it is the same duration experienced by the fatigued sample tested under 0.3% strain amplitude at 550 °C (including heating time 0.5 h, dwelling time 0.5 h, testing time 45.5 h, and cooling time 0.5 h).

3. Results and discussion

The quantitative TEM-EDX analysis of most grains in CoCrFeMnNi after LCF loading at 550 °C shows generally homogeneous distribution of alloying elements in the deformed sample with a concentration of (20 ± 3) at% for each element (not shown). However, additional secondary phases (with an irregular morphology and sizes varying up to a few μm) are observed close to grain boundaries. An example is presented in Fig. 1, where a HAADF STEM micrograph with EDX line scan (a) combined with a bright-field TEM image with SADP (b) of the same area are shown. The variation in the contrast along the secondary phase (in Figs. 1a and 1b) clearly indicates the change in chemical composition. The EDX line scan along the dashed line shows that the lower part of the secondary phase is Mn- and Ni-rich (area 1 in Fig. 1a) and the upper part is Cr-rich (area 2 in Fig. 1a).

Notably, the segregation induced NiMn-rich phases in post-annealed CoCrFeMnNi have been suggested to be tetragonal $L1_0$ NiMn phase [17–19]. Besides, the cosegregation of Ni and Mn at the grain boundary was mainly ascribed to the highly negative mixing enthalpy between Ni and Mn (and, on the other hand, the positive mixing enthalpy between Ni and Cr) [20]. This segregation induced $L1_0$ NiMn phase may also hold in the current CoCrFeMnNi, where both Ni and Mn elements have an atomic concentration of ca. 40%, see area 1 in Fig. 1.

Furthermore, the SADP from area 2 indicates that it has a tetragonal crystal structure with lattice parameters of a=b= 0.88 nm and c= 0.45 nm (space group P42/*mnm*), see Fig. 1b. Together with the EDX measurements in area 2, it is confirmed that the Cr-rich phase is the σ phase. This finding can also be supported by Fig. A1. This observation is consistent with the previous finding that the σ phase was observed in coarse-grained CoCrFeMnNi following prolonged exposure at 700 °C [21]. Besides, it should be mentioned that Cr-rich carbides (with carbon

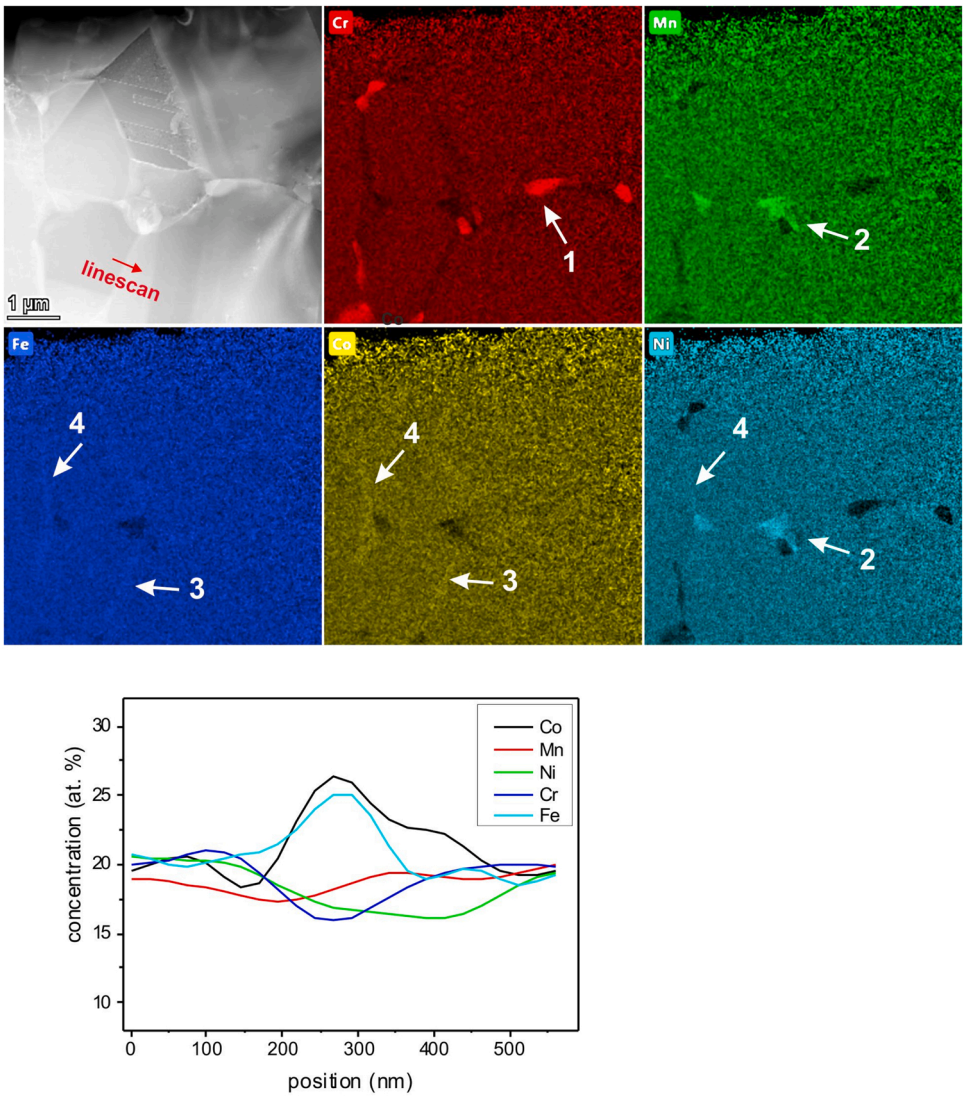

Fig. 2. HAADF STEM micrograph with the corresponding elemental composition EDX maps of the sample tested under strain amplitude of ± 0.3%. The areas marked by arrows are enriched in Cr (1), Mn-Ni (2) Fe-Co (3) and Ni (4). EDX line scan along the red arrow indicates Fe and Co segregation to grain boundary.

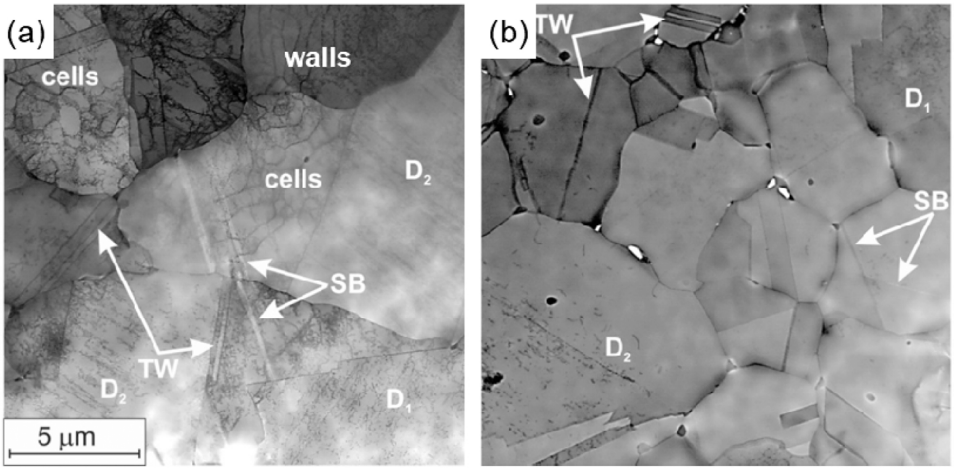

Fig. 3. Inverted HAAD STEM images of the samples after LCF under strain amplitudes of ± 0.75% (a) and ± 0.2% (b). D indicates dislocations. TW indicates annealing twins. D1 and D2 indicate discrete dislocations (D1) and pileup dislocations (D2). SB denotes slip bands. The scale bar in (a) is valid for (b).

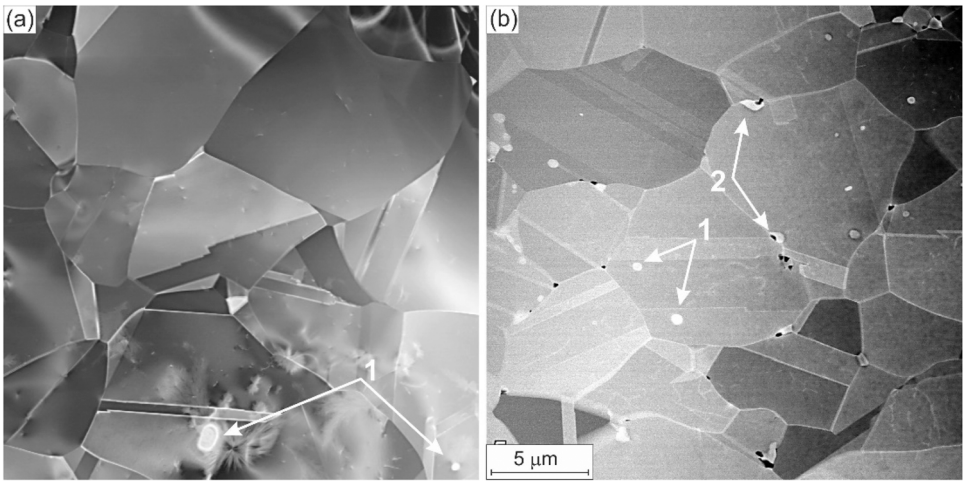

Fig. 4. HAAD STEM images of the samples without deformation, as-recrystallized at 800 °C for 1 h (a) and post-annealed at 550 °C for 47 h (b). Arrows marked secondary phases inside the grains (1) and at the grain boundaries (2). The scale bar in (b) is valid for (a).

contamination originating from the material processing steps) and Cr-rich body-centered cubic, BCC, phase were also reported in the CoCrFeMnNi after long-term annealing [18,21]. In this context, Cr-rich carbides (with the presence of carbon from processing steps) and BCC phases may also be presented in the current CoCrFeMnNi, which were not observed here, likely due to the limited investigated regions and requires further clarifications.

Apart from these Cr-rich and MnNi-rich secondary phases (*also see* region 1 and 2 in Fig. 2 with a lower magnification), the segregation of Fe, Co and Ni close to the grain boundary were also detected, see region 3 and 4 in Fig. 2. An EDX line scan along the red arrow indicates that the concentrations of Fe and Co are slightly increased to 25% (Fe) and 28% (Co) at the grain boundary, while the concentrations of Cr, Mn and Ni are decreased to around 15%. In other words, the concentration of Fe and Co is around 10% higher than those of Cr, Mn and Ni, which is higher than the general fluctuation level of the composition (~3%, see line scans in Figs. 1 and 2). Besides, the marked region 4 in Fig. 2 also shows increasing Fe-, Co and Ni-concentration and decreasing Cr- and Mn-concentration along the grain boundary. To our best knowledge, this is the first time reporting the segregation of the three elements close to grain boundaries of CoCrFeMnNi, which is in addition to previously reported FeCo cubic B2 phase [17,18]. Furthermore, the segregation of Fe, Co and Ni to the grain boundaries may be attributed to the lower negative enthalpy of mixing among these elements. For instance, the mixing enthalpy between Fe and Co was calculated to be − 2.9 kJ/mol, and the mixing enthalpy between Fe and Ni to be − 4.9 kJ/mol, which are comparable to that between Mn and Ni (−4.9 kJ/mol) [20].

It is of interest to note that the volume fraction of these secondary phases is estimated to be < 2%. It is worth mentioning that the secondary phases formation (such as carbides precipitation) was also observed in conventional FCC steels, such as 316LN steels, after intermediate-temperature fatigue and was reported to contribute to cyclic hardening [22]. In this work, these phases may also contribute to cyclic hardening, which may reduce the extent of cyclic softening that occurs due to dislocation cells/walls formation at high-to-medium strain amplitudes (see Fig. 3a) [23,24] (and finally contributed to a near-steady state).

It is of interest to compare the dislocation features from fatigued CoCrFeMnNi [15,16] to those from monotonic deformed CoCrFeMnNi [5]. Specifically, it was reported that at low monotonic strains upto 2.1%, the CoCrFeMnNi shows planar slip bands; whereas dislocations organized into cells at later stages (~20%) at RT and 600 °C [5]. These dislocation features are generally similar to that after fatigue loading, where slip bands and cell/wall structures (and tangles) dominated at low and high strain amplitudes, respectively, see Fig. 3a and b [15,16]. Differently, the average cell size after monotonic loading (~ in the range of 200–300 nm, from similar grain-sized CoCrFeMnNi [5]) is smaller than after fatigue loading (~ 1 μm, see Fig. 3a), due to the former's larger stress/strain levels (despite the latter's larger cumulative plastic strains). Besides, wall structures (and the evolution of persistent slip bands) are exclusively presented due to dislocations to-and-fro motion upon fatigue loading (i.e., not observed under monotonic loading). Additionally, dislocations to-and-fro motion may promote more point defects formation, such as vacancies, by dislocations cross-slip induced annihilation, as compared to that under monotonic loading.

On the other hand, when compared to that fatigued at RT, the dislocations movement at 550 °C may produce more thermally active vacancies, which may increase the extrusion height (and hence accelerate crack initiation). Therefore, more vacancies formation and their faster movement at 550 °C (along with grain boundary embrittlement due to secondary phases formation and *in-situ* oxidation [16]) contributed to the decreased fatigue lifetime as compared to RT.

Lastly, to further clarify the role of cyclic straining on the formation of the secondary phases, Fig. 4 shows the representative microstructures of the post-annealed sample at 550 °C for 47 h (without LCF loading). Notably, the microstructure of the recrystallized sample is also shown for comparison. In the as-recrystallized sample, round bright secondary phases with a low density (more arranged inside the grains, see arrows 1 in Fig. 4a) are observed. These are believed to be formed during material processing and mainly Cr-rich oxides [15]. For the post-annealed sample at 550 °C for 47 h, apart from the round-shape Cr-rich oxides (see arrow 1 in Fig. 4b) inside the grains, other secondary phases with an irregular morphology are observed at the grain boundaries (see arrow 2 in Fig. 4b). These secondary phases appear to have similar morphologies to those observed in the post-fatigued samples at 550 °C (Figs. 1 and 2) and are expected to have similar lattice structures.

Taking into account that no secondary phases form upon room temperature cyclic straining [23,24], it is suggested that elemental diffusion during high-temperature exposure (*e.g.*, at 550 °C) alone can facilitate the formation of Cr-and MnNi-rich secondary phases. This further suggests that cyclic straining may not play a decisive role in the precipitation of secondary phases but rather play an assisting role (because cyclic straining usually leads to the formation of vacancies, as mentioned above). Along with the aforementioned segregation's role in assisting grain boundary cracking, such segregation has to be considered in HEAs potential intermediate-temperature applications and attempts are needed by tuning HEAs to avoid it.

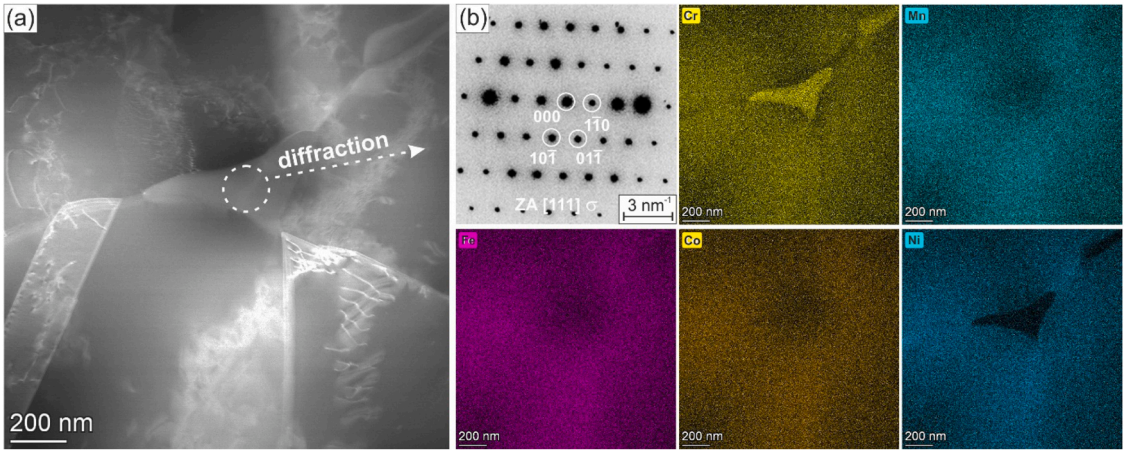

Fig. A1. (a) Cr-rich secondary phase with the corresponding elemental composition EDX maps of the CoCrFeMnNi tested under strain amplitude of ± 0.75%. (b) is the DP of the secondary phase from (a), indicated by the dashed circle. EDX maps and DP confirmed that the Cr-rich phase has σ phase structure.

4. Conclusion

In this study, the segregation of Fe, Co and Ni close to grain boundaries was observed in CoCrFeMnNi after intermediate-temperature (550 °C) cyclic loading. This finding is in addition to the previously reported precipitation of Cr-rich σ phase, BCC phase and carbide, MnNi $L1_0$ phase, as well as FeCo B2 phase. Further comparison to the post-annealed material (at 550 °C for 47 h, where similar precipitates also formed) suggests that cyclic straining play an assisting role in these phases' precipitation at elevated temperatures due to more vacancies formation. In addition, the difference of dislocation patterns betweencyclic loading and monotonic loading is also discussed, with more PSB-walls formed upon cyclic loading. Consequently, this work provides fresh understanding to the kinetic and cyclic deformation behaviors of the model CoCrFeMnNi HEA at intermediate temperatures.

CRediT authorship contribution statement

Dimitri Litvinov: Conceptualization, Formal analysis, Investigation, Methodology, Resources, Writing – original draft, Writing – review & editing. **Kaiju Lu:** Formal analysis, Investigation, Writing – original draft, Writing – review & editing. **Mario Walter:** Formal analysis, Investigation, Resources, Writing – review & editing. **Jarir Aktaa:** Conceptualization, Formal analysis, Investigation, Resources, Writing – review & editing.

Declaration of Competing Interest

The authors declare that they have no known competing financial interests or personal relationships that could have appeared to influence the work reported in this paper.

Data Availability

Data will be made available on request. The raw and processed data required to reproduce these findings are available on request to litvinov@kit.edu.

Acknowledgments

This work has been carried out within the framework of the Portfolio Research Project "Materials Research for the Future Energy Supply" of the Helmholtz Association of German Research Centers (HGF). The authors thank professor Martin Heilmaier (IAM-WK, KIT) and his co-workers for providing the material and their valuable comments on this work.

References

[1] B. Cantor, I.T.H. Chang, P. Knight, A.J.B. Vincent, Microstructural development in equiatomic multicomponent alloys, Mater. Sci. Eng.: A 375–377 (2004) 213–218, https://doi.org/10.1016/j.msea.2003.10.257.
[2] B. Gludovatz, A. Hohenwarter, D. Catoor, E.H. Chang, E.P. George, R.O. Ritchie, A fracture-resistant high-entropy alloy for cryogenic applications, Science 345 (6201) (2014) 1153–1158, https://doi.org/10.1126/science.1254581.
[3] E.P. George, W.A. Curtin, C.C. Tasan, High entropy alloys: a focused review of mechanical properties and deformation mechanisms, Acta Mater. 188 (2020) 435–474, https://doi.org/10.1016/j.actamat.2019.12.015.
[4] A.S. Tirunilai, J. Sas, K.-P. Weiss, H. Chen, D.V. Szabó, S. Schlabach, S. Haas, D. Geissler, J. Freudenberger, M. Heilmaier, A. Kauffmann, Peculiarities of deformation of CoCrFeMnNi at cryogenic temperatures, J. Mater. Res. 33 (19) (2018) 3287–3300, https://doi.org/10.1557/jmr.2018.252.
[5] F. Otto, A. Dlouhý, C. Somsen, H. Bei, G. Eggeler, E.P. George, The influences of temperature and microstructure on the tensile properties of a CoCrFeMnNi high-entropy alloy, Acta Mater. 61 (15) (2013) 5743–5755, https://doi.org/10.1016/j.actamat.2013.06.018.
[6] M.M. ZiJiao Zhang, Jiangwei Mao, Bernd Wang, Ze Gludovatz, Scott X. Zhang, Easo P. Mao, Qian George, Yu, O.Ritchie Robert, Nanoscale origins of the damage tolerance of the high-entropy alloy CrMnFeCoNi, Nat. Commun. 6 (2015) 10143, https://doi.org/10.1038/ncomms10143.
[7] Norihiko L. Okamoto, Shu Fujimoto, Yuki Kambara, Marino Kawamura, Zhenghao M.T. Chen, Hirotaka Matsunoshita, Katsushi Tanaka, Haruyuki Inui, Easo P. George, Size effect, critical resolved shear stress, stacking fault energy, and solid solution strengthening in the CrMnFeCoNi high-entropy alloy, Sci. Rep. 6 (2016) 35863, https://doi.org/10.1038/srep35863.
[8] W. Abuzaid, H. Sehitoglu, Critical resolved shear stress for slip and twin nucleation in single crystalline FeNiCoCrMn high entropy alloy, Mater. Charact. 129 (2017) 288–299, https://doi.org/10.1016/j.matchar.2017.05.014.
[9] G. Laplanche, A. Kostka, O.M. Horst, G. Eggeler, E.P. George, Microstructure evolution and critical stress for twinning in the CrMnFeCoNi high-entropy alloy, Acta Mater. 118 (2016) 152–163, https://doi.org/10.1016/j.actamat.2016.07.038.
[10] I.V. Kireeva, Yu.I. Chumlyakov, Z.V. Pobedennaya, I.V. Kuksgausen, I. Karaman, Orientation dependence of twinning in single crystalline CoCrFeMnNi high entropy alloy, Mater. Sci. Eng. A 705 (2017) 176–181, https://doi.org/10.1016/j.msea.2017.08.065.
[11] D.B. Miracle, O.N. Senkov, A critical review of high entropy alloys and related concepts, Acta Mater. 122 (2017) 448–511, https://doi.org/10.1016/j.actamat.2016.08.081.
[12] A.G. Wang, X.H. An, J. Gu, X.G. Wang, L.L. Li, W.L. Li, M. Song, Q.Q. Duan, Z. F. Zhang, X.Z. Liao, Effect of grain size on fatigue cracking at twin boundaries in a CoCrFeMnNi high-entropy alloy, J. Mater. Sci. Technol. 39 (2020) 1–6, https://doi.org/10.1016/j.jmst.2019.09.010.
[13] S. Sun, Y. Tian, H. Lin, H. Yang, X. Dong, Y. Wang, Z. Zhang, Transition of twinning behavior in CoCrFeMnNi high entropy alloy with grain refinement, Mater. Sci. Eng.: A 712 (2018) 603–607, https://doi.org/10.1016/j.msea.2017.12.022.
[14] S. Huang, W. Li, S. Lu, F. Tian, J. Shen, E. Holmström, L. Vitos, Temperature dependent stacking fault energy of FeCrCoNiMn high entropy alloy, Scr. Mater. 108 (2015) 44–47, https://doi.org/10.1016/j.scriptamat.2015.05.041.
[15] K. Lu, A. Chauhan, D. Litvinov, M. Walter, A.S. Tirunilai, J. Freudenberger, A. Kauffmann, M. Heilmaier, J. Aktaa, High-temperature low cycle fatigue

behavior of an equiatomic CoCrFeMnNi high-entropy alloy, Mater. Sci. Eng.: A 791 (2020), 139781.
[16] K. Lu, A. Chauhan, D. Litvinov, J. Aktaa, Temperature-dependent cyclic deformation behavior of CoCrFeMnNi high-entropy alloy, Int. J. Fatigue 160 (2022), 106863, https://doi.org/10.1016/j.ijfatigue.2022.106863.
[17] B. Schuh, F. Mendez-Martin, B. Völker, E.P. George, H. Clemens, R. Pippan, A. Hohenwarter, Mechanical properties, microstructure and thermal stability of a nanocrystalline CoCrFeMnNi high-entropy alloy after severe plastic deformation, Acta Mater. 96 (2015) 258–268.
[18] F. Otto, A. Dlouhý, K.G. Pradeep, M. Kuběnová, D. Raabe, G. Eggeler, E.P. George, Decomposition of the single-phase high-entropy alloy CrMnFeCoNi after prolonged anneals at intermediate temperatures, Acta Mater. 112 (2016) 40–52.
[19] M. Heczko, V. Mazánová, R. Gröger, T. Záležák, M.S. Hooshmand, E.P. George, M. J. Mills, A. Dlouhý, Elemental segregation to lattice defects in the CrMnFeCoNi high-entropy alloy during high temperature exposures, Acta Mater. 208 (2021).
[20] L. Li, R.D. Kamachali, Z. Li, Z. Zhang, Grain boundary energy effect on grain boundary segregation in an equiatomic high-entropy alloy, Phys. Rev. Materials 4 (2020), 053603.
[21] E.J. Pickering, R. Muñoz-Moreno, H.J. Stone, N.G. Jones, Precipitation in the equiatomic high-entropy alloy CrMnFeCoNi, Scr. Mater. 113 (2016) 106–109, https://doi.org/10.1016/j.scriptamat.2015.10.025.
[22] V.S. Srinivasan, M. Valsan, R. Sandhya, K. Bhanu Sankara Rao, S.L. Mannan, D. H. Sastry, High temperature time-dependent low cycle fatigue behaviour of a type 316L(N) stainless steel, Int. J. Fatigue 21 (1999) 11–21.
[23] K. Lu, A. Chauhan, M. Walter, A.S. Tirunilai, M. Schneider, G. Laplanche, J. Freudenberger, A. Kauffmann, M. Heilmaier, J. Aktaa, Superior low-cycle fatigue properties of CoCrNi compared to CoCrFeMnNi, Scr. Mater. 194 (2021), 113667.
[24] K. Lu, A. Chauhan, A.S. Tirunilai, J. Freudenberger, A. Kauffmann, M. Heilmaier, J. Aktaa, Deformation mechanisms of CoCrFeMnNi high-entropy alloy under low-cycle-fatigue loading, Acta Mater. 215 (2021), 117089.